

Topographical Scattering of Waves: Spectral Approach

R. Magne¹; F. Ardhuin²; V. Rey³; and T. H. C. Herbers⁴

Abstract: The topographical scattering of gravity waves is investigated using a spectral energy balance equation that accounts for first-order wave-bottom Bragg scattering. This model represents the bottom topography and surface waves with spectra, and evaluates a Bragg scattering source term that is theoretically valid for small bottom and surface slopes and slowly varying spectral properties. The robustness of the model is tested for a variety of topographies uniform along one horizontal dimension including nearly sinusoidal, linear ramp, and step profiles. Results are compared with reflections computed using an accurate method that applies integral matching along vertical boundaries of a series of steps. For small bottom amplitudes, the source term representation yields accurate reflection estimates even for a localized scatterer. This result is proved for small bottom amplitudes h relative to the mean water depth H . Wave reflection by small amplitude bottom topography thus depends primarily on the bottom elevation variance at the Bragg resonance scales, and is insensitive to the detailed shape of the bottom profile. Relative errors in the energy reflection coefficient are found to be typically $2h/H$.

DOI: 10.1061/(ASCE)0733-950X(2005)131:6(311)

CE Database subject headings: Surface waves; Scattering; Wave reflection; Spectral analysis; Topography.

Introduction

Wave propagation over any bottom topography can now be predicted with boundary element methods or other accurate numerical techniques. However, wave forecasting relies to a large extent on phase-averaged spectral wave models based on the energy or action balance equation (Gelci et al. 1957). For large bottom slopes waves can be reflected and this reflection is currently not represented in these models, while the significance of this process is still poorly known (Long 1973; Richter et al. 1976; Ardhuin et al. 2003). For waves propagating over a sinusoidal seabed profile, a maximum reflection or resonance is observed when the seabed wave number is twice as large as the surface wave wave number (Heathershaw 1982). Davies and Heathershaw (1984) proposed a deterministic wave amplitude evolution equation for normally incident waves over a sinusoidal seabed, based on a perturbation expansion for small bottom undulations. This theory was shown to be in good agreement with experimental data but overestimates reflection at resonance. Mei (1985) developed a more accurate

approximation, that is valid at resonance, using a multiple scale theory. This approach was further extended to a random bottom topography in one dimension (Mei and Hancock 2003). The Bragg resonance theory can be extended to any arbitrary topography, in two dimensions, that is statistically uniform (Hasselmann 1966). Ardhuin and Herbers (2002) further included slow depth variations. The resulting spectral energy balance equation contains a bottom scattering source term S_{bscat} , which is formally valid for small surface and bottom slopes and slowly varying spectral properties. S_{bscat} is readily introduced into existing energy-balance-based spectral wave models, and was numerically validated with field observations (Ardhuin et al. 2003). Although this stochastic theory is in a good agreement with deterministic results for small amplitude sinusoidal topography (Ardhuin and Herbers 2002), the assumed slowly varying bottom spectrum is not compatible with isolated bottom features, and the limitations and robustness of the source term approximation for realistic continental shelf topography are not well understood. The limitations of the stochastic source term model are examined here through comparisons with a deterministic model for arbitrary one-dimensional (1D) seabed topography that is uniform along the second horizontal dimension. We review the random Bragg scattering model, and investigate the applicability limits of the source term for a variety of seabed topography. Predicted reflection coefficients are compared with results based on Rey's (1992) model, which approximates the bottom profile as a series of steps. Examples include a modulated sinusoidal topography that is well within the validity constraints of the source term approximation as well as a steep ramp and a step that violate the assumption of a slowly varying bottom spectrum and thus provide a simple test of the robustness of the source term approximation.

¹Laboratoire de Sondages Electromagnétiques de l'Environnement Terrestre, Univ. de Toulon et du Var, BP 132, 83957 La Garde cedex, France and Centre Militaire d'Océanographie, Service Hydrographique et Océanographique de la Marine, 13, rue du Chatellier 29609 Brest cedex, France.

²Centre Militaire d'Océanographie, Service Hydrographique et Océanographique de la Marine, 13, rue du Chatellier 29609 Brest cedex, France.

³Laboratoire de Sondages Electromagnétique de l'Environnement Terrestre, Univ. de Toulon et du Var, 83957 La Garde cedex, France.

⁴Professor, Dept. of Oceanography, Naval Postgraduate School, Monterey, CA 93943.

Note. Discussion open until April 1, 2006. Separate discussions must be submitted for individual papers. To extend the closing date by one month, a written request must be filed with the ASCE Managing Editor. The manuscript for this paper was submitted for review and possible publication on February 5, 2004; approved on April 14, 2005. This paper is part of the *Journal of Waterway, Port, Coastal, and Ocean Engineering*, Vol. 131, No. 6, November 1, 2005. ©ASCE, ISSN 0733-950X/2005/6-311-320/\$25.00.

Theoretical Background

Matching Boundary Solution

We use Rey's (1992) algorithm, based on the theory of Takano (1960) and Kirby and Dalrymple (1983). It uses a decomposition

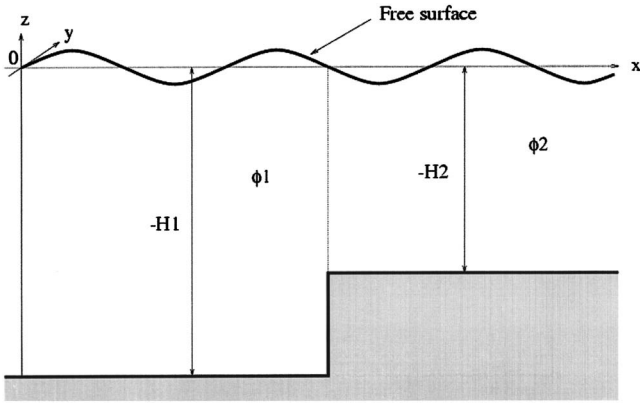


Fig. 1. Stepwise approximation

of the bottom profile in a series of N steps with integral matching along vertical boundaries between each pair of adjacent steps. A coordinate frame is defined with the horizontal x coordinate in the direction of the incident waves and the vertical z coordinate pointing upwards relative to the mean water level. The velocity potential is described by a sum of flat bottom propagating and evanescent modes. Evanescent modes are included in the matching condition to ensure a consistent treatment of the wave field (Rey 1992). The general solution of the velocity potential for a step (p) of depth H_p is given by the following equations:

$$\Phi_p(x, z, t) = \phi_p(x, z) e^{-i\omega p} \quad \text{for } p = 1, N \quad (1)$$

with

$$\phi_p(x, z) = \underbrace{A_p^\pm e^{\pm ikx} \chi_p(z)}_{\text{propagating modes}} + \sum_{q=1}^{\infty} \underbrace{B_{p,q}^\pm e^{\pm k_q x} \psi_{p,q}(z)}_{\text{evanescent modes}} \quad (2)$$

where $(\chi_p, \psi_{p,q} \quad q=1, \infty)$ define a complete orthogonal set for each step region (p)

$$\chi_p(z) = \cosh k_p(H_p + z) \quad (3)$$

$$\psi_{p,q}(z) = \cos k_{p,q}(H_p + z) \quad (4)$$

k_p and $k_{p,q}$ satisfy the following dispersion relations:

$$\frac{\omega_p^2}{g} = k_p \tanh(k_p H_p) \quad (5)$$

$$\frac{\omega_p^2}{g} = -k_{p,q} \tan(k_{p,q} H_p) \quad (6)$$

where g =acceleration of gravity.

Across each step (p), matching conditions between two domains (labeled $p=1$ and $p=2$ in Fig. 1) must be applied to ensure continuity of the fluid velocity and surface elevation

$$\phi_1 = \phi_2, \quad \frac{\partial \phi_1}{\partial x} = \frac{\partial \phi_2}{\partial x} \quad \text{for } -H_2 < z < 0 \quad (7)$$

$$\frac{\partial \phi_1}{\partial x} = 0 \quad \text{for } -H_1 < z < -H_2 \quad (8)$$

The integral formulation of these conditions (for $H_1 > H_2$) leads to

$$\int_0^{H_2} \phi_1 \chi_2 dz = \int_0^{H_2} \phi_2 \chi_2 dz \quad (9)$$

$$\int_0^{H_2} \phi_1 \psi_{2,q} dz = \int_0^{H_2} \phi_2 \psi_{2,q} dz \quad \text{for } q = 1, Q \quad (10)$$

$$\int_0^{H_1} \frac{\partial \phi_1}{\partial x} \chi_1 dz = \int_0^{H_2} \frac{\partial \phi_2}{\partial x} \chi_1 dz \quad (11)$$

$$\int_0^{H_1} \frac{\partial \phi_1}{\partial x} \psi_{1,q} dz = \int_0^{H_2} \frac{\partial \phi_2}{\partial x} \psi_{1,q} dz \quad \text{for } q = 1, Q \quad (12)$$

The orthogonality of the set functions largely simplifies these equations. In order to solve the problem numerically, the number of evanescent modes q are truncated to $q=Q$. Practically, only a few evanescent modes are needed to ensure convergence. For N steps, $2N(Q+1)$ equations are solved to obtain the $2N(Q+1)$ complex coefficients A_p^\pm and $B_{p,q}^\pm$. At the boundaries ($p=0$ and $p=N$), the reflection coefficient is given by

$$K_r = \frac{|A0^+|}{|A0^-|} \quad (13)$$

This method has the advantage that it is valid for arbitrary 1D topography.

Bragg Scattering Theory

We consider random waves propagating over a two-dimensional irregular bottom with a slowly varying mean depth H and small-scale topography h . The bottom elevation is given by $z = -H(\mathbf{x}) + h(\mathbf{x})$, with \mathbf{x} the horizontal position vector. The free surface position is $\zeta(\mathbf{x}, t)$.

Considering an irrotational flow for an incompressible fluid, we have the governing equations and boundary conditions for the velocity potential ϕ

$$\nabla^2 \phi + \frac{\partial^2 \phi}{\partial z^2} = 0 \quad \text{for } -H + h \leq z \leq \zeta \quad (14)$$

$$\frac{\partial \phi}{\partial z} = \nabla \phi \cdot \nabla(h - H) \quad \text{at } z = -H + h \quad (15)$$

$$\frac{\partial \zeta}{\partial t} = \frac{\partial \phi}{\partial z} \quad \text{at } z = \zeta \quad (16)$$

$$g\zeta + \frac{\partial \phi}{\partial t} = -\frac{1}{2} \left[|\nabla \phi|^2 + \left(\frac{\partial \phi}{\partial z} \right)^2 \right] \quad \text{at } z = \zeta \quad (17)$$

where ∇ and ∇^2 are the horizontal gradient and Laplacian operators. Eqs. (14)–(17) are, respectively, the Laplace's equation, free surface and bottom boundary conditions, and Bernoulli's equation. Combining these two last equations, we obtain

$$\frac{\partial^2 \phi}{\partial t^2} + g \frac{\partial \phi}{\partial z} = g \nabla \phi \cdot \nabla \zeta - \nabla \phi \cdot \frac{\partial \nabla \phi}{\partial t} - \frac{\partial \phi}{\partial z} \frac{\partial^2 \phi}{\partial t \partial z} \quad \text{at } z = \zeta \quad (18)$$

Assuming that the surface and the small-scale bottom slopes are of the same order ε , and the large-scale bottom slope is of order ε^2 , a perturbation expansion of ϕ up to the third order in ε yields

the following spectral energy balance equation (details are given in Ardhuin and Herbers 2002):

$$\frac{dE(\mathbf{k}, \mathbf{x}, t)}{dt} = S_{\text{bscat}}(\mathbf{k}, \mathbf{x}, t) \quad (19)$$

where

$$S_{\text{bscat}}(\mathbf{k}, \mathbf{x}, t) = K(k, H) \int_0^{2\pi} \cos^2(\theta - \theta') F^B(\mathbf{k} - \mathbf{k}', \mathbf{x}) \times [E(\mathbf{k}', \mathbf{x}, t) - E(\mathbf{k}, \mathbf{x}, t)] d\theta' \quad (20)$$

with

$$K(k, H) = \frac{4\pi\omega k^4}{\sinh(2kH)[2kH + \sinh(2kH)]} \quad (21)$$

$E(\mathbf{k}, \mathbf{x}, t)$ is the surface elevation spectrum and $F^B(\mathbf{k}, \mathbf{x})$ is the small-scale bottom elevation spectrum. These spectra are slowly varying functions of (\mathbf{x}, t) and \mathbf{x} , respectively. \mathbf{k} is the wave number vector defined by $\mathbf{k} \equiv (k \cos \theta, k \sin \theta) \equiv (k_x, k_y)$, where θ defines the angle with the x axis. The spectral densities E and F^B are defined such that the integral over the entire \mathbf{k} plane equals the local variance

$$\langle h^2(\mathbf{x}) \rangle = \int_{-\infty}^{+\infty} \int_{-\infty}^{+\infty} F^B(\mathbf{k}, \mathbf{x}) dk_x dk_y \quad (22)$$

The frequency ω is given by the dispersion relation

$$\omega^2 = gk \tanh(kH) \quad (23)$$

Here we consider a steady wave field in one dimension with incident and reflected waves propagating along the x axis. After integration over k_y , k_x becomes k and Eq. (19) reduces to

$$C_g \frac{\partial E(k, x)}{\partial x} + C_k \frac{\partial E(k, x)}{\partial k} = S_{\text{bscat}}(k, x) \quad (24)$$

with a source term

$$S_{\text{bscat}}(k, x) = K(h, H) \frac{F^B(2k, x)}{k} [E(-k, x) - E(k, x)] \quad (25)$$

The first term of Eq. (24) represents advection in physical space with the group velocity defined by

$$C_g = \frac{dx}{dt} = \frac{\partial \omega}{\partial k} \quad (26)$$

and the second term describes the effect of shoaling on the wave number

$$C_k = \frac{dk}{dt} = -C_g \frac{2k^2}{2kh + \sinh(2kh)} \frac{\partial H}{\partial x} \quad (27)$$

Reflection by Modulated Sinusoidal Bottom Topography

The source term approximation was validated by Ardhuin and Herbers (2002) for random waves reflecting from a sinusoidal seabed, by integrating S_{bscat} analytically across the wave spectrum in the limit of weak reflection [$E(-k) \ll E(k)$, with positive and negative wave numbers corresponding to the incident and reflected waves, respectively]. A comparison with Dalrymple and Kirby's (1986) solution gave good agreement, even for only a few

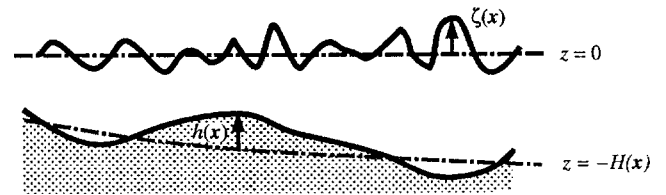


Fig. 2. Definitions

bars. For stronger reflection, Eq. (24) is not readily evaluated analytically, and numerical integration is not feasible since a sinusoidal bottom has an infinitely narrow spectrum (a Dirac distribution), and thus cannot be represented with a finite bottom discretization Δk_b .

We consider instead a bottom spectrum with a finite width that corresponds to a modulated sinusoidal bottom profile. The modulated seabed is represented by a sum of cosines

$$h(x) = \sum_{i=-(m-1)/2}^{i=(m-1)/2} b_i \cos[(k_{b,0} + i\Delta k_b)x] \quad (28)$$

The slowly varying depth (H), defined in Fig. 2 is taken constant whereas the perturbation (h) represents the modulated seabed. We define the root-mean-square bar amplitude b from the bottom variance, $b = \sqrt{\langle h^2 \rangle}$, and a representative bottom slope $\varepsilon = bk_{b,0}$. The reflected wave energy is calculated for the bed profile shown in Fig. 3, with the peak bottom wave number $k_{b,0} = 6 \text{ m}^{-1}$ ($\lambda_{b,0} = 1.04 \text{ m}$), and a short modulation length with $m=3$, and equal amplitudes (b_i) for all bottom components. The length of the bed is 1.5 modulation lengths, giving the bottom spectrum shown in Fig. 4. The reflection from this modulated sinusoidal bottom was evaluated for an incident Pierson–Moskowitz spectrum, with a peak at k_0 satisfying the Bragg resonance condition $2k_0 = k_{b,0}$ (Fig. 5). Spectral results for Rey's model were obtained by evaluating reflection coefficients for monochromatic waves over a range of frequencies and integrating the reflected energy across the spectrum. Seventy steps are used to resolved the bathymetry. Results for various values of b are displayed in the form of reflection coefficients R (Fig. 6) as a function of the slope $bk_{b,0}$. R is defined by the ratio of the reflected and incident energies: $R = (\sum_{k<0} E) / (\sum_{k>0} E)$. Predictions based on the source term

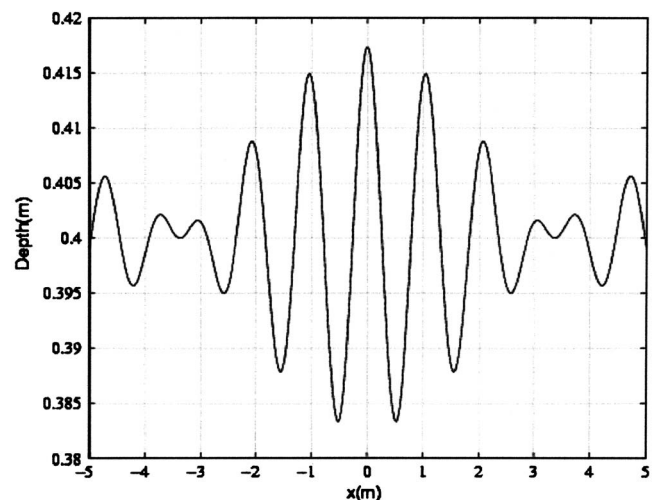


Fig. 3. Modulated seabed ($m=3$), $bk_{b,0}=0.06$

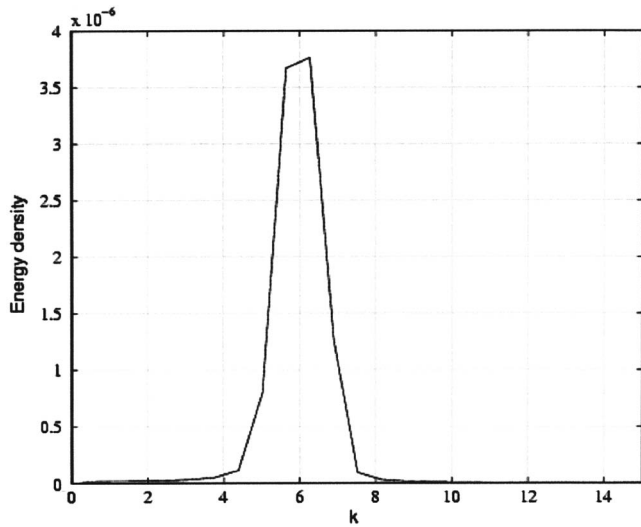


Fig. 4. Modulated seabed spectrum ($m=3$)

method (R_{Smod}) and the matching boundary model using five evanescent modes (R_{MBmod}) agree well over a wide range of bottom slopes. The solutions gradually diverge for large bottom slopes where the source term underpredicts the reflection. Even for $bk_0=0.3$ ($b/\lambda_0=0.05$), differences are less than 10% confirming the robustness of the source term method for steep topography.

To evaluate the effect of the spectral width on the reflection coefficient, Fig. 6 also includes predictions for sinusoidal topography ($m=0$) with the same variance. Results for sinusoidal topography were obtained using Mei's (1985) analytical approximation and Rey's (1992) algorithm. The resulting reflection coefficients R_{Mei} and R_{MBsin} , respectively, agree for small bottom slopes (Fig. 6) and diverge for larger slopes as already shown by Rey (1992). Indeed, R_{Mei} was derived for small bottom slopes while the matched boundary solution converges to the exact reflection for any bottom profile when the number of evanescent modes goes to infinity. What may seem surprising is that the reflection coefficient for the sinusoidal and modulated sinusoidal topographies R_{MBmod} and R_{MBsin} agree for small slopes although bottom profiles are quite different. Apparently, for small bottom

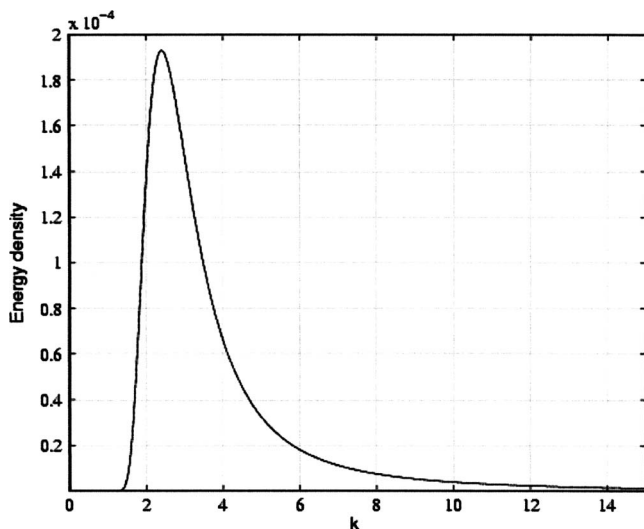


Fig. 5. Incident wave spectrum

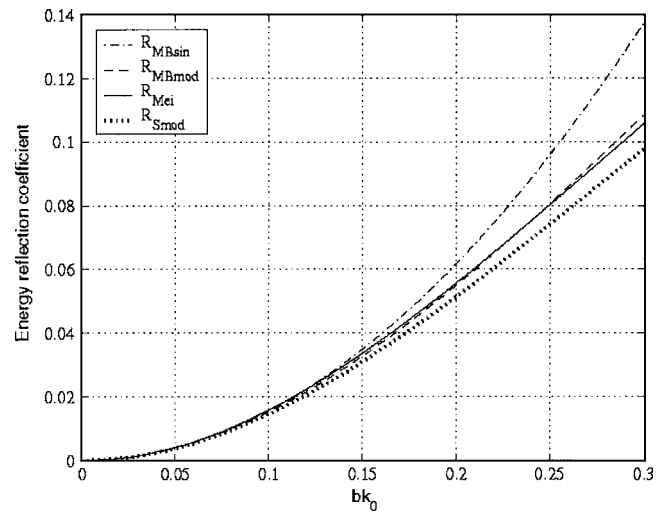


Fig. 6. Wave reflection by modulated sinusoidal bottom

slopes and narrow bottom spectra the reflection is only a function of the total bottom elevation variance b^2 and does not depend on the phases of its components. This result is obvious from the viewpoint of the source term theory that was derived for small bottom slopes, and does not retain the phases of the bottom spectrum components. The predicted reflection depends on the convolution of the wave spectrum with the bottom spectrum at the Bragg resonance wave number [the integral of Eq. (25) over all wave numbers]. If the bottom spectrum is narrow compared with the wave spectrum then the total source term depends only on the total bottom variance and the surface spectral density at the Bragg resonance wave number.

Reflection by a Linear Ramp

To investigate the robustness of the variance-based source term model for reflection induced by localized topography, we consider the linear ramp problem used in previous studies to test the mild slope equation (Booij 1983). In the source term approximation, wave scattering is the result of interactions between surface waves and bottom variations at the scale of the surface wavelength. The scattering model is thus based on a decomposition of the topography into a slowly varying depth H and a perturbation h (small-scale topography), which corresponds to a separation between refraction and shoaling that occurs over the slowly varying depth H and scattering at these short scales. For practical applications, it is desirable to have a perturbation h that is zero outside of a finite region, so that the spectrum of h is well defined. Once the two criteria that the slope of H does not exceed a given threshold and h is zero outside of a region of radius nL are satisfied, the choice of the depth decomposition in h and H is fairly arbitrary and does not affect the following results. For simplicity we take a piecewise linear function for $H(x)$, so that the perturbation $h(x)$ takes the form of a triangular wave (Fig. 7).

The ramp profile is defined by the fixed water depths H_1, H_2 , whereas the ramp slope α is varied by adjusting its length $2L$ (Fig. 7). To ensure that $H(x)$ is slowly varying, γ has to be small. This is achieved by extending the domain to a length $2nL$ with $n > 1$ (Fig. 7). The slope of H is then given by $\tan \gamma = (\tan \alpha)/n$, with several values of n tested below.

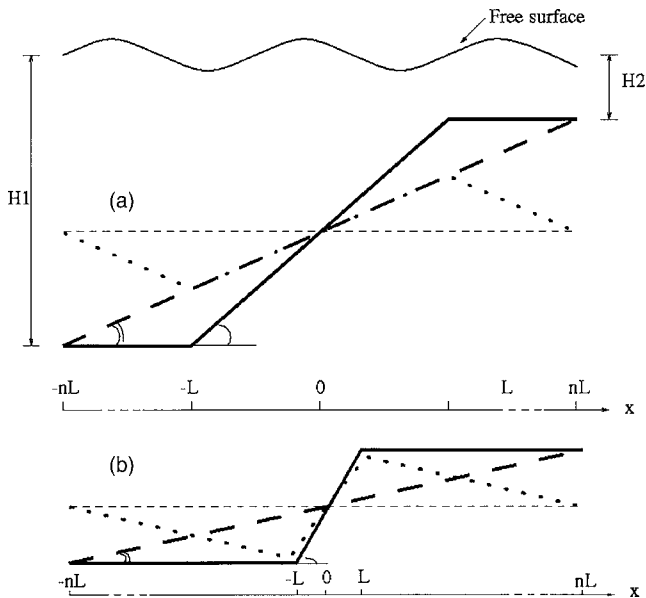


Fig. 7. Decomposition of linear ramp (solid line) into a slowly varying depth H (dashed line) and residual h (dotted line); (a) and (b) for small and large n , respectively

First Test Case: Small Depth Change

We first consider a ramp with a small depth transition from $H_1=0.5$ to $H_2=0.3$ m. The incident wave spectrum is represented by the same Pierson–Moskowitz spectrum that was used in the previous section with the peak wave number in deep water $k_0=3$ m⁻¹ (Fig. 5), so that $k_0H_1=1.5$ and $k_0H_2=0.9$. In order to investigate the source term applicability limits, the linear ramp slope $\tan \alpha$ is varied from 0.01 to 2.9. For each value of α , several values of γ are tested, with n varying from 5 to 50. The reflection coefficient R_S (source term reflection due to the residual) is compared with the “exact” computation R_{MB} (matching boundary algorithm) in Fig. 8 and the relative error $(R_S - R_{MB})/R_{MB}$ is shown in Fig. 9. In our calculations, for slopes of H such as $\tan \alpha < 0.4$, $R_{S,n=5}$ is within 30% of the exact value R_{MB} . For larger values of $\tan \alpha$, $R_{S,n=5}$ decreases and tends to zero (Fig. 8),

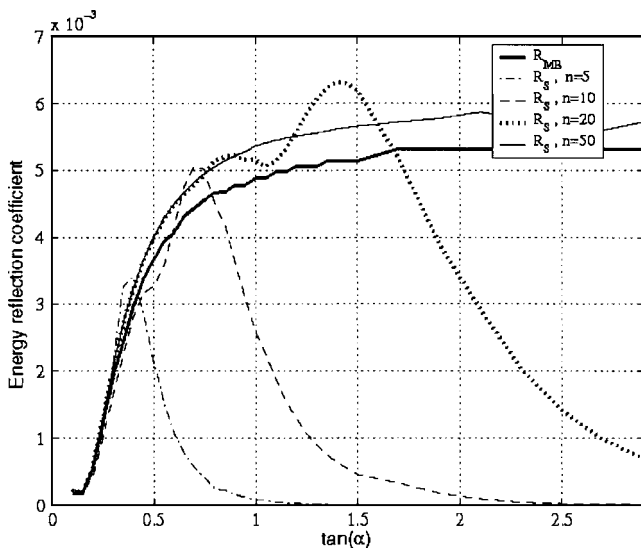


Fig. 8. Wave reflection by a ramp

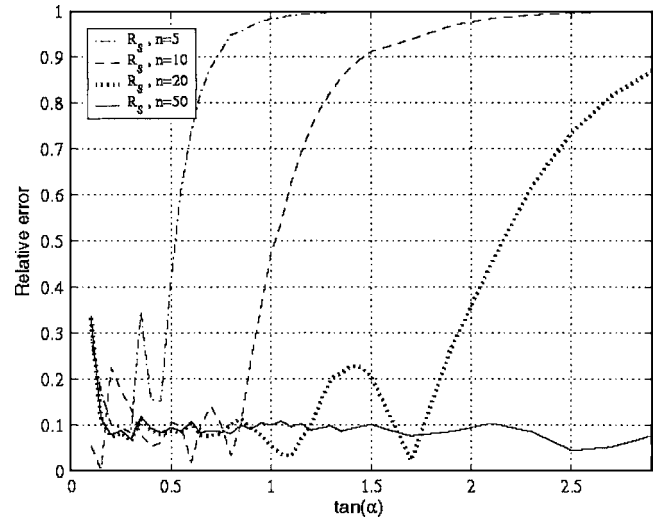


Fig. 9. Relative errors in wave reflection by a ramp

whereas the exact solution R_{MB} converges to the reflection over a vertical step as $\tan \alpha$ goes to infinity. The value $\tan \alpha=0.4$ corresponds to $\tan \gamma (= \tan \alpha/5)$ equal to 0.08. For larger n the slope of H is reduced and $R_{S,n}$ is valid for a wider range of ramp slopes.

We notice that for all values of n shown in Fig. 8, the model gives reasonable results for $\tan \gamma [= (\tan \alpha)/n]$ up to about 0.08. The ramp slope does not appear to be a limiting factor (as it was assumed in the theory). For $\tan \gamma$ larger than 0.08 the reflection is increasingly underestimated probably because of the contribution of the large-scale profile $H(x)$ to the reflection.

As n increases h approaches the slope of the actual ramp and $R_{S,n}$ converges to $R_{S,\infty}$ which is about 10% larger than R_{MB} for all ramp slopes. As discussed in the following, the accuracy of the model is apparently not limited by the ramp slope.

It may seem surprising that $R_{S,n}$ actually converges for large n whereas the bottom spectrum does not. In the case of a vertical step of height h in the middle of a domain of length $2nL$, the spectral density $F^B(k)$ of a discrete variance spectrum of the residual is proportional to $h^2/2nLk^2$ and tends to zero (except around $k=0$) as n goes to infinity. However the source term formulation represents scattering as uniformly distributed along the bottom, and the integration of the source term along the wave propagation path yields a reflection that is proportional to $2nL F^B(k)$ and thus converges when n goes to infinity. The use of infinite support for H and h (taking the limit $n \rightarrow \infty$) to compute the reflection over a localized ramp is counterintuitive. It represents a physically localized scattering with a mathematically distributed source. In practice, the bottom spectrum is obtained by discrete Fourier transform of the bottom, and it only tends to continuous power spectrum in the limit $n \rightarrow \infty$. Further, it should be realized that the bottom power spectrum is the Fourier transform of the bottom autocovariance function used by Mei and Hancock (2003, see the Appendix).

For a nonrandom bottom such as the ramp here, one may use intermediate results by Mei and Hancock (2003) where the hypothesis that the bottom is random only comes in for discarding nonlinear wave effects (which are not taken into account here). It thus appears that our rather surprising result for the convergence as $n \rightarrow \infty$ is justified by the convergence of the discrete spectrum to the continuous power spectrum and the theory of Mei and Hancock (2003) applied to nonrandom bottoms (see the Appendix). It shows that the far field scattered energy by small ampli-

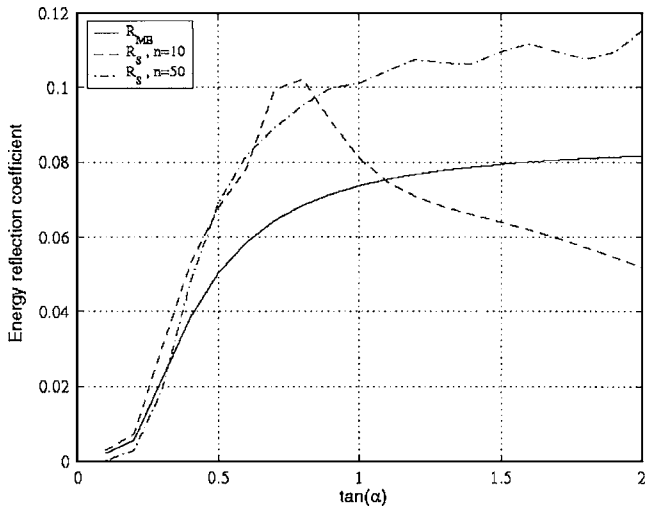


Fig. 10. Wave reflection by Booiij's ramp

tude depth variations only depends on the power spectrum of the scatterers at the Bragg scale, and not on its localization in space, as long as the bottom amplitude remains small.

Booiij's Ramp: Larger Depth Change

This approach should clearly break down for finite bottom amplitudes, in particular because subharmonic scattering was observed (Belzons et al. 1991) whereas it is not explained by the present theory. Such a limit should be tested to see whether our present approach has some practical applicability. We therefore take a second test case with a larger ramp is taken from Booiij (1983) with water depths $H_1=4.97$ m, $H_2=14.92$ m, and an incident wave peak period $T=10$ s. The corresponding peak wave number in deep water $k_0=0.04$ m⁻¹ so that $k_0H_1=0.6$ and $k_0H_2=0.2$. Results for ramp slopes $\tan \alpha$ ranging from 0.001 to 2.9, and $n=10$ and 50 are shown in Fig. 10.

We notice again that $R_{S,n}$ converges for large n , provided that $(\tan \alpha)/n < 0.08$. However, in this case the relative error is larger than in the first test case, up to about 30%. The two tests have the same ramp slopes but different ratio of water depths at the edges of the ramp $H_1/H_2=3$ here versus $H_1/H_2=1.7$ in the previous case. The two cases suggest that the source term is more sensitive to the amplitude than the slope of the bottom perturbation h . Formally, the bottom amplitude only appears in the bottom boundary condition (15), which is linearized at $z=-H$ using the following Taylor series expansion:

$$\Phi|_{z=-H+h} = \Phi|_{z=-H} + h \frac{\partial \Phi}{\partial z}|_{z=-H} + \frac{h^2}{2} \frac{\partial^2 \Phi}{\partial z^2}|_{z=-H} + O(h^3) \quad (29)$$

Ardhuin and Herbers (2002) use a representative length scale $1/k_0$ to nondimensionalize Eq. (29) as

$$\tilde{\Phi}|_{\tilde{z}=-H+h} = \tilde{\Phi}|_{\tilde{z}=-H} + \eta \frac{\partial \tilde{\Phi}}{\partial \tilde{z}}|_{\tilde{z}=-H} + \frac{\eta^2}{2} \frac{\partial^2 \tilde{\Phi}}{\partial \tilde{z}^2}|_{\tilde{z}=-H} + O(\eta^3) \quad (30)$$

where $\tilde{z}=k_0z$, $\eta=k_0h$, η corresponding to the scales that cause wave scattering. The validity of the Taylor expansion requires that η is small and also that the first and second derivative of $\tilde{\Phi}$ with respect to \tilde{z} are of order 1. In this approximation (30) is limited by the small-scale slope k_0h . However one may also take H_0 as the representative length which leads to the same Eq. (30) with

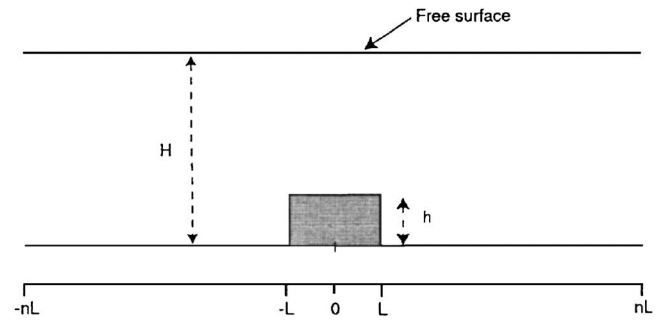


Fig. 11. Sketch of the step

$\eta=h/H_0$, limited then by the water depth ratio h/H_0 . The choice of the representative length was arbitrary and can be justified only a posteriori, by evaluating the scale of variation of Φ and thus the magnitude of $\partial \tilde{\Phi} / \partial \tilde{z}$ and $\partial^2 \tilde{\Phi} / \partial \tilde{z}^2$. The numerical results presented here show that the source term is more sensitive to the water depth change h/H_0 than the small-scale slope k_0h . Booiij (1983) had found that the standard mild slope equation (Berkhoff 1972) gave errors less than 10% for $\tan \alpha$ up to 1/3. Our results suggest that the Bragg scattering model can be as accurate as the mild slope equation for computing reflection, but only for $\Delta h/H_0$ less than 0.2.

Reflection by a Step

Now that the effect of h/H_0 is well established, one may question the importance of other parameters. We thus evaluate source term predictions of broad and narrow surface wave spectra over steps of varying height to gain further insight into the limitations of the source term approximation for localized topography. Reflection of waves by a rectangular step has been investigated analytically and experimentally in numerous studies (Neuman 1965a,b; Miles 1967; Mei and Black 1969; Mei 1983; Rey et al. 1992) and is well understood. The step is defined in Fig. 11, where $2L$ is the step-length, h is the height, and $2nL$ is the size of the entire computational domain.

Numerical Setup

The spectral density of the bottom $F^B(k)$ is proportional to $h^2/2nLk^2$. Hence, integration of the source term along the wave propagation path yields a reflection that is proportional to $2nLF^B(k) \sim h^2/k^2$, independent of n . Although the domain length has not effect on real waves in the absence of bottom friction, it influences the discretization of the bottom spectrum ($\Delta k=2\pi/2nL$), and thus it may have an impact on the numerical results. However $2nF^B(n)$ converges as n goes to infinity (Fig. 12), so that the domain length does not change the results for large enough values of n . A large domain with $n=8$ was used here.

The step width ($2L$) is taken to be half the wavelength of the surface waves for a spectrum peak $k_{op}=0.04$ m⁻¹ ($L_0=157$ m) in a water depth of 15 m. Two different wave spectra are used here (bold lines in Fig. 12): a wide spectrum (solid) with a classic Pierson-Moskowitz shape, typical of wind seas, and the narrow swell-like spectrum (dashed) with a Gaussian shape. Once the

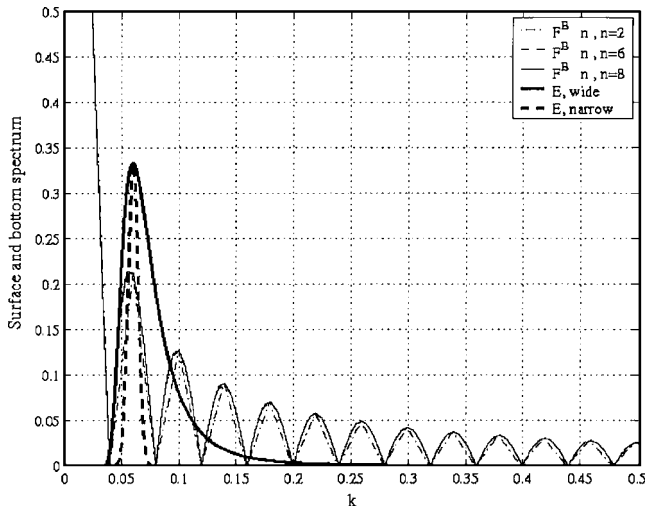


Fig. 12. Wide and narrow surface wave spectra superposed on the bottom spectrum for domain sizes $n=2, 6,$ and 8 . The bottom spectrum is rescaled by the surface wave number $[F^B(k/2)]$ to show the resonant bottom and surface components.

shape of wave spectrum is chosen, the solution is a function of three nondimensional variables: the step height h/H , the water depth $k_{op}H$, and the relative step width $k_{op}L$.

Influence of the Height of the Step

The accuracy of the source term for a range of nondimensional step heights h/H is evaluated in intermediate and shallow water through comparison with the exact matching boundary algorithm (Fig. 13). Energy reflection coefficients are compared for two different water depths, $k_{op}H=0.1$ and $k_{op}H=0.6$, representative of shallow and intermediate depths. The incident wave spectrum has a Pierson–Moskowitz shape.

As expected from previous calculations, the error in the source term increases with the step amplitude h/H . For $h/H < 0.05$ the

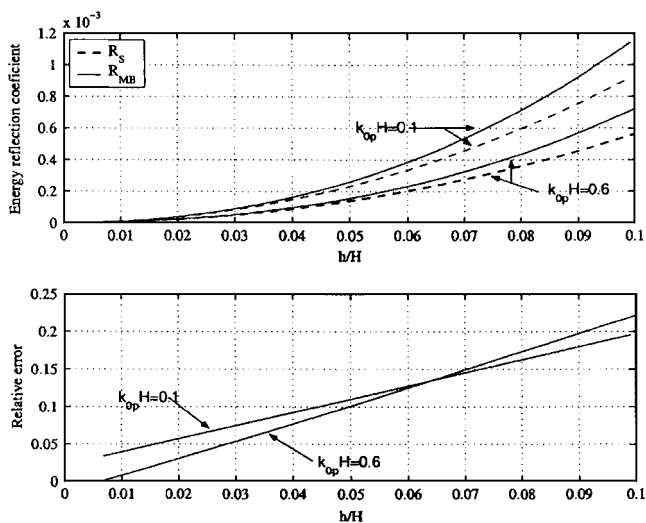


Fig. 13. Reflected energy computed with the source term (dashed line) and with the matching boundary algorithm (solid line), for intermediate depth ($k_{op}H=0.6$) and shallow water ($k_{op}H=0.1$), and relative error of the source term

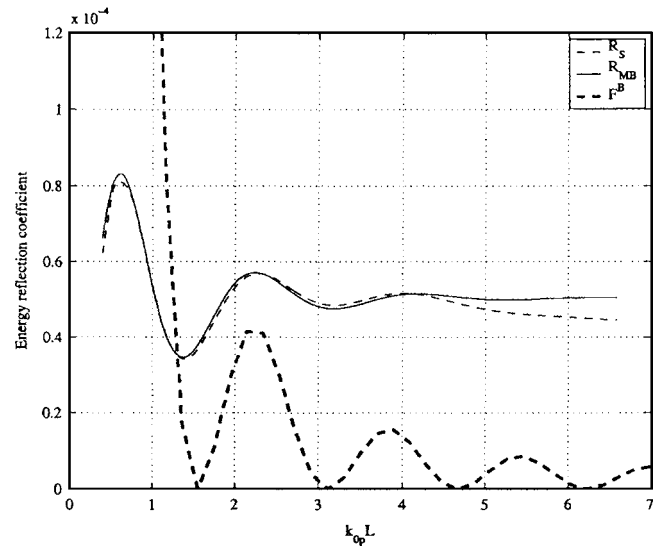


Fig. 14. Reflected energy computed with the source term (dashed line) and with the matching boundary algorithm (solid line) for a wide wave spectrum. The bottom spectrum (F^B) is also indicated, scaled by the normalized resonant surface wave number to indicate the resonant response (bold dashed line). Other parameters are $h/H=0.02$ and $k_{op}H=0.1$.

error in the predicted reflection coefficients is less than 10%. These results provide further confirmation that the height of the localized scatterer is a limiting factor for the source term computation, but not its slope, which is infinite here, and this result holds for very shallow water.

Influence of the Width of the Step and the Wave Spectrum

Here we consider the dependence of the reflection coefficient on the width of the step and the width of the wave spectrum for a small amplitude step ($h/H=0.02$) in shallow water ($k_{op}H=0.1$). The nondimensional step width $k_{op}L$ is varied, effectively changing the position of the wave spectrum peak relative to the bottom spectral peaks (see Fig. 12). Results are shown in Figs. 14 and 15 for wide and narrow wave spectra, respectively. The same computation is done for the narrow spectrum (Fig. 15).

For both wide and narrow surface waves spectra, the source term yields accurate results, and the errors do not appear to be sensitive to the width of the step. Oscillations in the reflection coefficient with varying $k_{p0}L$ represent an interference phenomenon that has been described in numerous previous studies. When a monochromatic incident wave runs up the leading edge of the step at $x=-L$, it is partly reflected and partly transmitted. As the transmitted component passes the rear edge of the step at $x=L$, it is again partially reflected and partially transmitted. If the reflected waves originating from the front and rear edges of the step are in phase we have a constructive interference which amplifies the reflection. Conversely, destructive interference occurs if the two reflected wave trains are 180° out of phase and cancel out, yielding zero reflection. For long waves, maximum reflection occurs when $\sin^2 2k_{p0}L=1$ (Mei 1983), where k_{p0} is the incident wave wave number. This condition is met when

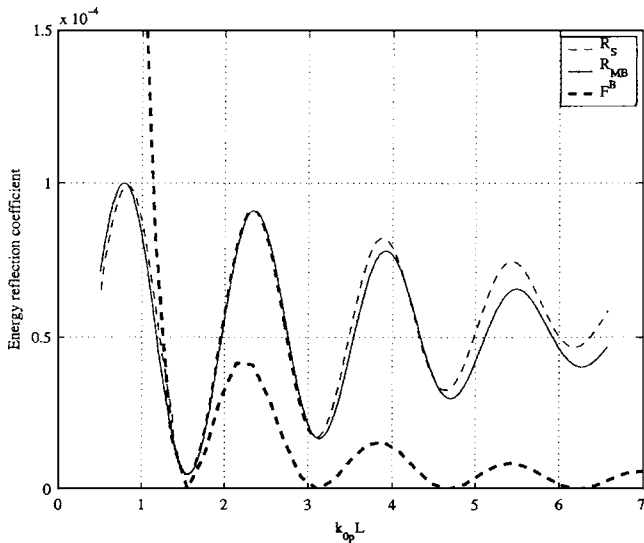


Fig. 15. Same as Fig. 14 but for a narrow wave spectrum

$$2k_{p0}L = (2n - 1)\frac{\pi}{2}, \quad n = 1, 2, 3, \dots \quad (31)$$

The corresponding values of $k_{p0}L$ are $k_{p0}L = \pi/4 \approx 0.78$, $3\pi/4 \approx 2.35$, $5\pi/4 \approx 3.93$, These values match with the reflection peaks observed in Figs. 14 and 15 both for the source term and the matching boundary algorithm. In the wide spectrum case (Fig. 14) these oscillations are suppressed and for high values of $k_{p0}L$, the reflection tends to a constant value. Using Bragg scattering, this is explained by the fact that in the limit of large step width $k_{p0}L$ the wave spectrum is wider than the side lobes of the bottom spectrum (see Fig. 12) and the effects of constructive and destructive interferences for different spectral component average out. The reflection coefficient is a convolution of the bottom spectrum and the surface wave spectrum, and thus the reflection is insensitive to bottom spectral details with scales finer than the wave spectrum width.

Conclusions

Predictions of the scattering of surface waves by bottom topography based on a spectral energy balance equation that includes a wave-bottom Bragg scattering source term (Ardhuin and Herbers 2002) are compared with exact results based on a matching boundary algorithm (Rey 1992). The source term yields accurate reflection predictions for modulated sinusoidal topography. In the limit of small bottom amplitudes h compared to the water depth H , the two models yield identical results, confirming that the far-field scattered wave is determined entirely by the variance spectrum of the bottom and does not depend on the phases of its components. This finding also holds for localized topography, a result that can be justified by the approach of Mei and Hancock (2003) using their intermediate results for nonrandom bottoms. In that case, the bottom spectrum must be carefully calculated over a large enough domain in order to resolve the important bottom scales. Using discrete Fourier transforms, one may use an artificial gently sloping extension of the area covered by scatterers. However, it is found that it also holds for very steep topography, such as a single step, for a variety of water depths and wave spectrum shapes, as long as $h < H$ is small. In our calculations,

relative errors in the energy reflection coefficient are found to be typically $2h/H$, or h/H for the amplitude reflection coefficient. These results show that the Bragg scattering source term is a reasonably accurate method for representing wave reflection in spectral wave models, for a wide range of small amplitude bottom topographies found on continental shelves. The source term approach is also very efficient compared to the elliptic models such as proposed by Athanassoulis and Belibassakis (1999). An extension of the source term to higher order (e.g., following Liu and Yue 1998) may reduce errors for larger values of h/H , that are shown here to be the limiting factor in practical applications. Results for 1D bottom profiles are expected to hold for practical 2D applications of the source term approximation.

Acknowledgments

This research is supported by a joint grant from the Centre National de la Recherche Scientifique (CNRS) and Délégation Générale pour l'Armement (DGA). Additional funding is provided by the U.S. Office of Naval Research, and the U.S. National Science Foundation in the framework of the 2003 Nearshore Canyon Experiment (NCEX). Fruitful discussions with Kostas Belibassakis are gratefully acknowledged.

Appendix. Reconciliation of Random and Deterministic Wave Theories

Mei and Hancock (2003) considered the same problem of a wave train propagating over an arbitrary topography of small amplitude h . In their scaling h is small compared to the wavelength $2\pi/k$, but, as discussed in this paper, the scaling for the bottom perturbation could also be the mean water depth H . These writers further assume that h is a random function that is stationary with respect to the fast coordinate x , and introduce a slow coordinate x_1 for variations in the statistics of h . This two-scale approach is similar to that used by Arduin and Herbers (2002). Mei and Hancock (2003) obtained an amplitude evolution equation in which the topography acts as a linear damping with a coefficient β_i given by their Eq. (B8) as

$$\beta_i = \frac{\omega(k\sigma)^2 k(\hat{\gamma}(2k) + \hat{\gamma}(0))}{4 \cosh^2 kH(\omega^2 H/g + \sinh^2 kH)} \quad (32)$$

where $\sigma^2(x_1)\gamma =$ autocorrelation function of the bottom topography, decomposed in a slowly varying local variance $\sigma^2(x_1)$ and a normalized autocovariance γ . $\hat{\gamma}$ is the Fourier transform of γ . Although Mei and Hancock's (2003) result does not conserve energy (which requires the introduction of higher order terms, see Arduin and Herbers 2002), it is rather general as far as the bottom is concerned. The essential difference with Arduin and Herbers (2002) is that there is no need for a large number of bottom undulations to obtain an expression for the scattering, and the "number of undulations" is properly defined by the scale over which the bottom autocovariance goes to zero.

Naturally the two theories are consistent, and we can obtain from β_i the damping coefficient β_E for the energy, which is twice that for the wave amplitude A since $\partial(AA^*)/\partial t = -2\beta_i AA^* = -\beta_E AA^*$, with A^* the complex conjugate of A . Rewriting Eq. (32) one has

$$\beta_E = \frac{2k^3 \omega \sigma^2 (\hat{\gamma}(2k) + \hat{\gamma}(0))}{\sinh 2kH [2kH + \sinh 2kH]} \quad (33)$$

For a zero-mean stationary process the Fourier transform of the autocovariance function is simply 2π times the power spectral density F^B (e.g., Priestley 1981, theorem 4.8.1, p. 211), so that, for $F^B(0)=0$, we get

$$\beta_E = \frac{4\pi k^3 \omega F^B(2k)}{\sinh 2kH [2kH + \sinh 2kH]} \quad (34)$$

which is the linear part of the bottom scattering source term (25) in one dimension

$$S_{\text{bscat}}(k) = \beta_E (E(-k) - E(k)) \quad (35)$$

Interestingly the hypothesis of randomness for h is not important for the value of β_i when averaged over the entire field of scatterers (however, it does impact the real part, i.e., the phase of the waves). Following Mei and Hancock's (2003) derivation, one may define a β_i that is also a function of the fast coordinate x using their Eq. (2.36), and in that case the derivation is identical, replacing $\sigma^2(x_1)\gamma$ by $h(x)h(x-\xi)$, all the way to their Eqs. (B1)–(B3). Then one may define a mean value, which, in the case of a finite region with scatterers between $-nL$ and nL reads

$$\bar{\beta}_i = \frac{1}{2nL} \int_{-nL}^{nL} \beta_i(x) dx \quad (36)$$

Taking the imaginary part of their Eqs. (B1)–(B3) we have

$$\bar{\beta}_i = \omega \frac{k^2}{2 \cosh^2(kH)} \left\{ \frac{I_0}{\omega^2 H/g + \sinh^2(kH)} + \sum_{n=1}^{\infty} \frac{k I_n}{k_n [\omega^2 H/g + \sinh^2(k_n H)]} \right\} \quad (37)$$

with

$$I_0 = -\Re \left\{ \frac{1}{2nL} \int_{-nL}^{+nL} \int_{-\infty}^{+\infty} \left(\frac{d^2}{d\xi^2} - ik \right) (h(x)h(x-\xi)) e^{ik\xi + ik_n|\xi|} d\xi dx \right\} \quad (38)$$

and

$$I_n = -\Im \left\{ \frac{1}{2nL} \int_{-nL}^{+nL} \int_{-\infty}^{+\infty} \left(\frac{d^2}{d\xi^2} - ik \right) (h(x)h(x-\xi)) e^{ik\xi + ik_n|\xi|} d\xi dx \right\} \quad (39)$$

Switching the order of the integrals, Eqs. (38) and (39) are identical to their equations (B2) and (B3), provided that we redefine γ as the full autocovariance function

$$\gamma(\xi) = \frac{1}{2nL} \int_{-nL}^{+nL} h(x)h(x-\xi) dx \quad (40)$$

In this case γ is obviously real and even and we obtain their Eq. (B8) for $\bar{\beta}_i$.

We have thus proved that in one dimension and in the limit of small bottom amplitudes the scattering source term applies to nonrandom bottoms. In these conditions, the linear part of the source term represents the damping of the incident waves (and thus also the scattered wave energy) averaged over the area covered by scatterers.

Notation

The following symbols are used in this paper:

- A = propagating modes amplitude;
- B = evanescent modes amplitude;
- b = root-mean-square amplitude from the bottom variance;
- C_g = group velocity;
- C_k = spectral advection velocity;
- E = surface elevation spectral density;
- F^B = small-scale bottom elevation spectrum;
- H = water depth;
- h = bottom perturbation height;
- K = source term coefficient;
- K_r = amplitude reflection coefficient;
- k = surface wave number;
- $k_{b,0}$ = peak bottom wave number;
- k_0 = peak wave number in deep water;
- k_{0p} = peak wave number;
- L = half-length of the ramp;
- L_0 = peak wavelength;
- m = modulation parameter;
- n = mild slope inclination parameter;
- R = energy reflection coefficient;
- R_{MB} = matching boundary energy reflection coefficient;
- R_{Mei} = Mei energy reflection coefficient;
- R_S = source term energy reflection coefficient;
- S_{scat} = bottom scattering source term for the wave energy spectrum;
- T_0 = peak period;
- α = ramp inclination;
- γ = mild slope inclination;
- Δk_b = discretization of the bottom spectrum;
- ε = representative bottom slope;
- ζ = free surface position;
- η = small parameter;
- Φ = velocity potential;
- χ, ψ_n = complete orthogonal set of functions; and
- ω = wave radian frequency.

Subscripts

- \sim = nondimensionalized variable.

References

- Ardhuin, F., and Herbers, T. H. C. (2002). "Bragg scattering of random surface gravity waves by irregular seabed topography." *J. Fluid Mech.*, 451, 1–33.
- Ardhuin, F., Herbers, T. H. C., Jessen, P. F., and O'Reilly, W. C. (2003). "Swell transformation across the continental shelf. Part II: Validation of a spectral energy balance equation." *J. Phys. Oceanogr.*, 33, 1940–1953.
- Athanassoulis, G. A., and Belibassakis, K. A. (1999). "A consistent coupled-mode theory for the propagation of small amplitude water waves over variable bathymetry regions." *J. Fluid Mech.*, 389, 275–301.
- Belzons, M., Rey, V., and Guazzelli, E. (1991). "Subharmonic bragg resonance for surface water waves." *Europhys. Lett.*, 16(2), 189–194.
- Berkhoff, J. C. W. (1972). "Computation of combined refraction-diffraction." *Proc., 13th Int. Conf. on Coastal Engineering*, ASCE, Vancouver, B.C., Canada, 796–814.
- Booij, N. (1983). "A note on the accuracy of mild-slope equation." *Coastal Eng.*, 7, 191–203.

- Dalrymple, R. A., and Kirby, J. T. (1986). "Water waves over ripples." *J. Waterw., Port, Coastal, Ocean Eng.*, 112(2), 309–319.
- Davies, A. G., and Heathershaw, A. D. (1984). "Surface-wave propagation over sinusoidally varying topography." *J. Fluid Mech.*, 144, 419–443.
- Gecli, R., Cazalé, H., and Vassal, H. (1957). "Prévision de la houle, la méthode des densités spectroangulaires." *Bulletin d'information du Comité central d'Océanographie et d'Etude des Côtes*, 9, 416–435.
- Hasselmann, K. (1966). "Feynman diagrams and interaction rules of wave-wave scattering processes." *Rev. Geophys.*, 4, 1–32.
- Heathershaw, A. D. (1982). "Seabed-wave resonance and sand bar growth." *Nature (London)*, 296, 343–345.
- Kirby, J. T., and Dalrymple, R. A. (1983). "Propagation of obliquely incident water waves over a trench." *J. Fluid Mech.*, 133, 47.
- Liu, Y., and Yue, D. K. P. (1998). "On generalized Bragg scattering of surface waves by bottom ripples." *J. Fluid Mech.*, 356, 297–326.
- Long, B. (1973). "Scattering of surface waves by an irregular bottom." *J. Geophys. Res.*, 78(33), 7861–7870.
- Mei, C. C. (1983). *Applied Dynamics of Ocean Surface Waves*, Wiley-Interscience.
- Mei, C. C. (1985). "Resonant reflexion of surface water waves by periodic sandbars." *J. Fluid Mech.*, 152, 315–335.
- Mei, C. C., and Black, J. L. (1969). "Scattering of surface waves by rectangular obstacles in water of finite depth." *J. Fluid Mech.*, 38, 499–515.
- Mei, C. C., and Hancock, M. J. (2003). "Weakly nonlinear surface waves over a random seabed." *J. Fluid Mech.*, 475, 247–268.
- Miles, J. W. (1967). "Surface-wave scattering matrix for a shelf." *J. Fluid Mech.*, 28, 755–767.
- Neuman, J. N. (1965a). "Propagation of water waves over a infinite step." *J. Fluid Mech.*, 23, 399–415.
- Neuman, J. N. (1965b). "Propagation of water waves past long two-dimensional obstacles." *J. Fluid Mech.*, 23, 23–30.
- Priestley, M. B. (1981). *Spectral analysis and time series*, Academic Press, London.
- Rey, V. (1992). "Propagation and local behaviour of normally incident gravity waves over varying topography." *Eur. J. Mech. B/Fluids*, 11, 213–232.
- Rey, V., Belzons, M., and Guazzelli, E. (1992). "Propagation of surface gravity waves over a rectangular submerged bar." *J. Fluid Mech.*, 235, 453–479.
- Richter, K., Schmalfeldt, B., and Siebert, J. (1976). "Bottom irregularities in the North Sea." *Deut. Hydrogr. Z.*, 29, 1–10.
- Takano, K. (1960). "Effets d'un obstacle parallélépipédique sur la propagation de la houle." *Houille Blanche*, 15, 247.